Optimising flow and mixing in a full-scale gas-mixed anaerobic digester by integrating sludge rheological data using computational fluid dynamics

Wei, Peng; Uijttewaal, Wim; Spanjers, Henri; van Lier, Jules B.; de Kreuk, Merle

Important note
To cite this publication, please use the final published version (if applicable).
Please check the document version above.

Optimising flow and mixing in a full-scale gas-mixed anaerobic digester by integrating sludge rheological data using computational fluid dynamics

Peng Wei [a,b,*], Wim Uijttewaal [c], Henri Spanjers [a], Jules B. van Lier [a], Merle de Kreuk [a]

[a] *Delft University of Technology, Department of Water Management, Stevinweg 1, 2628 CN Delft, the Netherlands*
[b] *Delft University of Technology, Department of Chemical Engineering, van der Maasweg 9, 2629 HZ Delft, the Netherlands*
[c] *Delft University of Technology, Department of Hydraulic Engineering, Stevinweg 1, 2628 CN Delft, the Netherlands*

ABSTRACT

Gas-mixing is commonly applied in anaerobic digesters, yet the resulting flow and hydraulic mixing are difficult to evaluate because of limited full-scale experimental data and uncertainties in integrating sludge rheological data. This study used computational fluid dynamics (CFD) to assess the impact of treated sludge rheology on flow and mixing characterisation in a full-scale biogas-mixed digester. The CFD model, which was firstly validated using a lab-scale setup, showed that flow and mixing predictions depended on the rheological properties, especially at low shear rates. The predicted dominant shear rate was out of the effective shear-rate range of the Ostwald model, leading to flow and mixing performance overestimation. The results indicated that there are limitations in applying the Ostwald model and the conventional approaches for determining dead-zone. The Herschel-Bulkley model was more appropriate for the prevailing low shear rates and predicted large viscosity gradients in the digester, indicating two distinct compartments with different flow and mixing behaviour based on the gas-sparging height: a plug-flow compartment with dominant vertical convection above, and a dead-zone compartment with considerable segregation below. The results showed that the applied gas-sparging induced insufficient flow and mixing, but contributed to the well-functioning of the digester. To correctly assess flow and mixing, the applied rheological data should be in agreement with the type of sludge that is treated in the digester. Our results indicate that the shear rate in the digester must be increased and various options for achieving this are proposed.

1. Introduction

Effective anaerobic digestion performance relies on good mixing to benefit transfer and interaction between substrates and biomass. In anaerobic digesters that are designed as a continuous stirred tank reactor (CSTR), good mixing needs to be achieved by auxiliary equipment. Commonly, recirculation of produced biogas or gas-mixing is used [1]. However, achieving sufficient mixing is usually challenging in full-scale installations, resulting in relatively low operational performance in practice. In such case, troubleshooting of the operational system should rely on clear evaluation of the gas-mixing performance. Although the applied gas flow rate is known, evaluating the actual degree of mixing is very difficult in an opaque digester. Thus far, only few studies have

reported experimental evaluation using a tracer test in full-scale digesters [2,3]. In these studies, the reactors are mixed by sludge recirculation and the obtained flow and mixing characteristics are limited. As a widely-used numerical approach, computational fluid dynamics (CFD) has been applied to gas-mixed digesters, yet most developed models are applied to lab-scale reactors [4–9]. In the few models applied to full-scale digesters, the gas-mixing implemented by bottom-mounted nozzle(s) closely resembled a bubble-column pattern [10–12].

Sludge rheology is found to be a significant influencing factor in design and operation of sludge treatment processes [13,14]. It has also been considered in some CFD studies, and the integrated rheological data are commonly characterised by the Ostwald or power-law model [3,7,9,11,15–17] and the Herschel-Bulkley model [11,12]. Results of the full-scale simulations have revealed a considerable rheological impact

---

on sludge flow predictions [10–12]. However, the referred rheological data are originally from manure slurry [18,19]. The manure slurry has distinct rheological properties compared to sewage sludge from municipal wastewater treatment plants (WWTP), which has been characterised in our previous studies [20,21]. Hence, for further application in any other full-scale installation, the rheological discrepancy in sludge types or sources should be considered. Moreover, the potential changes in predicted flow and mixing performance are also unclear, which have not been investigated yet. The considerable rheological impact on the gas-mixed flow reported in our lab-scale model [9], needs to be further assessed in a full-scale digester. From a practical point of view, a better insight into the correlation between sludge rheology and flow/mixing is also important to propose straightforward and concrete solutions for troubleshooting and optimisation of process performance in full-scale reactors.

This study focused on a full-scale anaerobic digester equipped with a number of vertical lances, through which a recycled biogas flow was injected into the digester. Since the nature of the digester makes
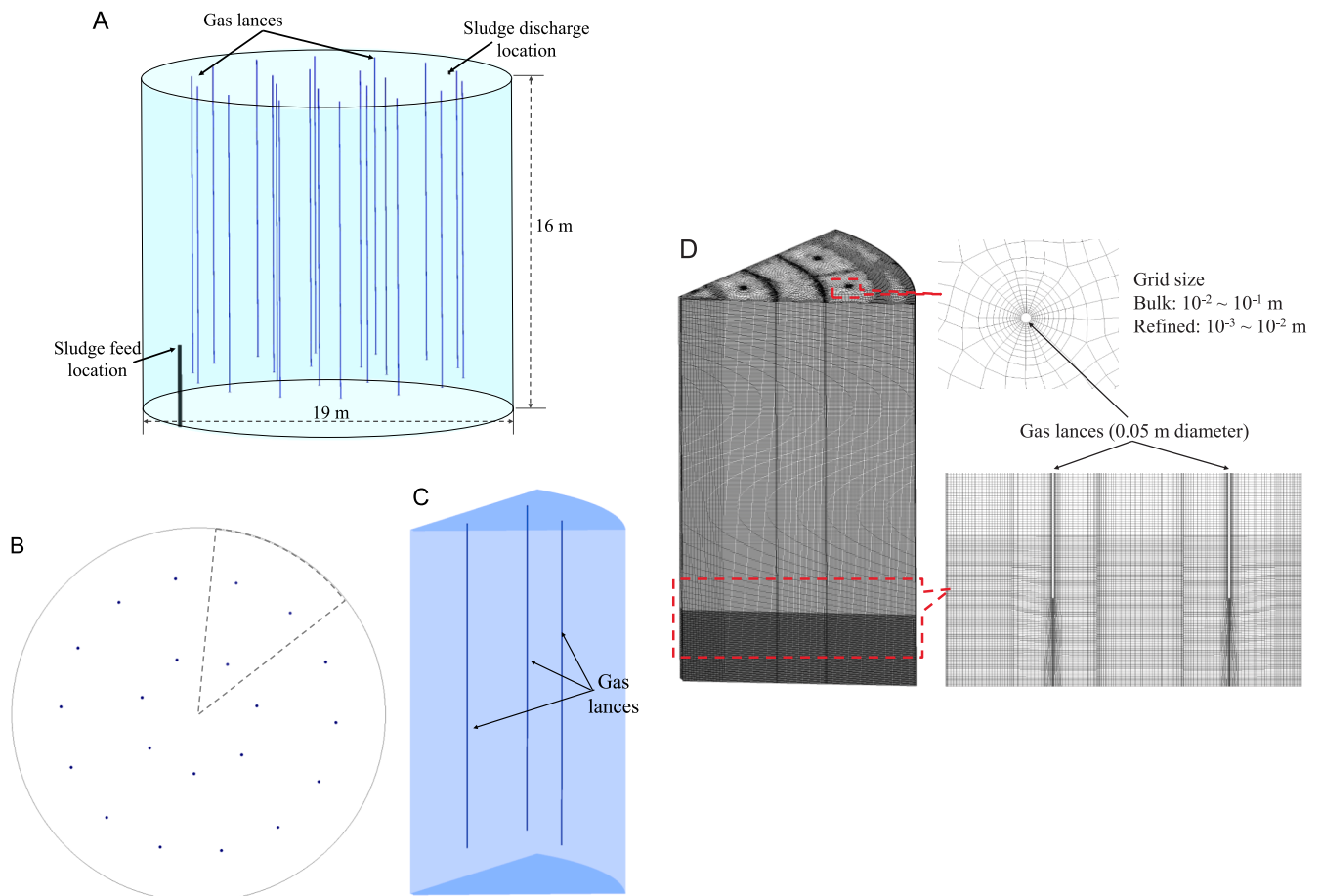

Fig. 1. (A) Geometry, and (B) top view of the full-scale anaerobic digester; (C) geometry, and (D) mesh of the computational domain.

experimenting and data-collection problematic, CFD modelling was applied to characterise the resulting flow and mixing in the digester. Assuming that the important processes are represented in this physics-based approach, a sensitivity analysis can reveal shortcomings and directions for improvement. The study aims to 1) assess the applicability and sensitivity of the applied rheological models, including Ostwald and Herschel-Bulkley, on sludge flow and mixing characteristics; 2) assess the flow and mixing performance induced by the applied gas-mixing operation; and 3) propose recommendations or guidelines for optimisation and design in practice.

2. Model setup

2.1. Geometry, computational domain and mesh

The studied anaerobic digester is located at WWTP De Groote Lucht (The Netherlands). As shown in Fig. 1A, the cylindrical digester has a designed effective volume of 4560 m^3, with 19 m diameter and 16 m height. The semi gas-lift pattern is implemented using a gas-sparging system with 21 gas lances. Each gas lance has 5 cm inner-diameter and is vertically located with a clearance of 1.75 m from the tank bottom. Fig. 1B shows a top view of the 21 gas lances: 7 and 14 gas lances are evenly distributed to form an inner circle and an outer circle, respectively. The digester is operated with a solids retention time of 27 days. Preliminary simulations showed a negligible effect of the sludge feeding velocity on the overall flow in the digester (data not shown). To focus on the gas-sparging process, a simplified computational domain without the feeding process was developed, based on the regular geometry and layout (the dashed sector in Fig. 1B). As shown in Fig. 1C, the domain represents 1/7 of the whole digester, and contains three gas lances in accordance with the segmented layout of the digester cross section. Regular hexahedron grids were created in the whole domain; local mesh refinement was applied in regions in close vicinity to the gas lances (Fig. 1D), whose diameter (5 cm) was largely different with the tank (19 m). The optimal mesh containing 4.67 million grid cells was determined for simulations, based on a convergence study with four characteristic grid sizes from coarse to fine (details described in Supplementary A).

2.2. Model development

2.2.1. Two-phase model

Our simulations were implemented using the commercial package ANSYS-Fluent, mainly on a Dell Precision 7910 computer with Intel Xeon E5-2630 processor and 64 GB RAM. An Eulerian-Eulerian model was applied to solve for the two-phase mass and momentum balances, in which both liquid and gas phases were assumed as a continuum. The sludge was set to the liquid phase, and the biogas, assumed as a mixture of CH$_4$ and CO$_2$, was set to the gas phase. Physical properties of the biogas were proportional to the defined volume fractions of CH$_4$ (75%) and CO$_2$ (25%), which slightly differed from commonly observed values in sewage sludge digesters [22]. These proportional changes were found to have negligible effects on the two-phase flow predictions, so any volume fraction discrepancy in biogas between the model setting and reality was not considered. Drag force, lift force, and turbulent dispersion force were involved to characterise the gas–liquid interaction. Turbulence was simulated based on the Reynolds-Averaged-Navier-Stokes (RANS) method, and the RNG (Re-normalisation group) k-ε model [23] was applied. Details of all the governing equations and models are consistent with our lab-scale model setup [9]. Potential bubble shape changes due to enlarged bubble sizes were considered. Thus, different bubble shapes were involved, and the Grace model [24] was applied to calculate the drag force on a single bubble:

$$C_D = \alpha_l \cdot max\big(C_{D\_sphere},\ min\big(C_{D\_ellipse}, C_{D\_cap}\big)\big) \tag{1}$$

where C_D denotes the drag coefficient, and α_l is the liquid volume fraction. The $C_{D\_ellipse}$, C_{D_cap} and C_{D_sphere} correlate to specific bubble shapes, and are defined as

$$C_{D\_sphere} = \begin{cases} \dfrac{24}{Re_g} & Re_g \leqslant 0.01 \\[2ex] \dfrac{24 \cdot \big(1 + 0.15 \cdot Re_g^{0.687}\big)}{Re_g} & Re_g > 0.01 \end{cases} \tag{2}$$

$$C_{D\_cap} = \frac{8}{3} \tag{3}$$

$$\begin{cases} C_{D\_ellipse} = \dfrac{4}{3} \cdot \dfrac{g \cdot d_g \cdot (\rho_l - \rho_g)}{U_t^2 \cdot \rho_l} \\[2ex] U_t = \dfrac{\mu_l}{\rho_l \cdot d_g} \cdot Mo^{-0.149} \cdot (J - 0.857) \\[2ex] J = \begin{cases} 0.94 \cdot H^{0.757} & 2 < H \leqslant 59.3 \\ 3.42 \cdot H^{0.441} & H > 59.3 \end{cases},\ H = \dfrac{4}{3} \cdot Eo \cdot Mo^{-0.149} \cdot \left(\dfrac{\mu_l}{0.0009}\right)^{-0.14} \end{cases} \tag{4}$$

where Re_g denotes the relative Reynolds number based on the relative velocity between the two phases:

$$Re_g = \frac{\rho_l \cdot |\vec{v}_g - \vec{v}_l| \cdot d_g}{\mu_l} \tag{5}$$

Mo is the Morton number

$$Mo = \frac{g \cdot (\rho_l - \rho_g) \cdot \mu_l^4}{\rho_l^2 \cdot \sigma^3} \tag{6}$$

and *Eo* is the Eötvös number

$$Eo = \frac{g \cdot (\rho_l - \rho_g) \cdot d_g^2}{\sigma} \tag{7}$$

where, g denotes the gravitational acceleration, d is the diameter, ρ is the density, $\vec{v}$ is the velocity, and σ is the surface tension coefficient. The subscript l and g refer to the primary phase (liquid) and the secondary phase (gas), respectively.

2.2.2. Rheological model

Rheological data of the studied sludge were characterised by two widely used rheological models: the Ostwald model (Equation (8)) and the Herschel-Bulkley model (Equation (9)).

$$\mu = K \cdot \gamma^{n-1} \tag{8}$$

$$\mu = \frac{\tau_0}{\gamma} + K \cdot \gamma^{n-1} \tag{9}$$

where μ denotes the sludge apparent viscosity, K is the flow consistency index, γ is the shear rate, n is the flow behaviour index, and τ_0 is the yield stress.

2.2.3. Tracer simulation and mixing assessment

Tracer simulations were carried out to assess mixing performance. The tracer was set to have the same physical properties as the sludge, with a molecular diffusion coefficient of 1×10^{-9} m^2/s. Turbulent diffusivity was determined by the calculated turbulent viscosity and the turbulent Schmidt number (0.7). To characterise the mixing performance in the entire domain, the tracer was initially concentrated in a small sphere (0.5 m radius) and released from the domain top. Tracer dispersion was calculated by the transport equation:

$$\frac{\partial}{\partial t}(\alpha_l \cdot \rho_l \cdot c_{tc}) + \nabla \cdot (\alpha_l \cdot \rho_l \cdot c_{tc} \cdot \vec{v}_l - \alpha_l \cdot \rho_{tc} \cdot D_{tc} \cdot \nabla c_{tc}) = 0 \tag{10}$$

where t denotes time, c is the tracer concentration, and D is the diffusion coefficient including the molecular and turbulent diffusivity. The subscripts l and tc refer to the liquid phase and the tracer, respectively. The mixing performance was assessed using coefficient of variance (CoV) of the tracer concentration. All grid cells in the domain were involved to calculate CoV [25,26]

$$CoV = \sqrt{\frac{\sum_{i=1}^{N}\left(\left(\frac{c_i - c_m}{c_m}\right)^2 \cdot V_i\right)}{\sum_{i=1}^{N} V_i}} \qquad (11)$$

where c_i denotes the tracer concentration in grid cell i, c_m is the volume-average tracer concentration, V_i is the liquid volume in grid cell i, and N is the total number of grid cells. Mixing degrees were specified by CoV values, e.g., CoV of 0.75 represents the 75% mixing degree. The 95% mixing degree (CoV of 0.05) was used as the ideal mixing threshold. It should be noted that the liquid flux crossing the periodic planes was negligible, thus the periodicity assumption was expected to have a negligible impact on the tracer's dispersion throughout the computational domain from top to bottom, which could represent the overall mixing performance in the whole digester.

2.3. Boundary conditions and simulation settings

Regarding the simplified domain, a periodic boundary condition was applied for the two rectangular side planes. The domain top was set to a degassing boundary to discharge gas and retain liquid. The end side of the gas lances was set to velocity inlet for gas. All other boundaries were set to a wall condition with no-slip for liquid and free-slip for gas.

Time step sizes were set based on the Courant-Friedrichs-Lewy condition, and the 1st order implicit scheme was applied for transient simulations. The Phase Coupled SIMPLE (Semi-implicit method for pressure linked equations) scheme was used for pressure–velocity coupling. The 3rd order QUICK (Quadratic interpolation for convective kinetics) scheme [27] was applied for the momentum equations, and the 1st order upwind scheme for the volume fraction, turbulence, and tracer transport equations. Convergence was obtained when all residuals reached an order of 10^{-4}, and the gas phase obtained a balance between the gas inlet and the degassing top (mass imbalance $< 5\%$).

3. Results and discussion

3.1. Sludge rheological characterisation and model validation

Fig. 2 shows that both Ostwald and Herschel-Bulkley models provided a good fit to the measured rheological data of the studied sludge. Generally, estimated model parameters are valid in a specified shear rate (γ) range, in which the minimum shear rate (γ_{min}) correlates to the maximum apparent viscosity (μ_{max}), and vice versa (for $0 < n < 1$). In the Ostwald model, constant apparent viscosity μ is assumed out of the effective range; in the Herschel-Bulkley model, μ out of the effective range ($< \gamma_{min}$) is calculated by [28]

$$\mu = \frac{\tau_0}{\gamma_{min}} \cdot \left(2 - \frac{\gamma}{\gamma_{min}}\right) + K \cdot \gamma_{min}^{n-1} \cdot \left(2 - n + \frac{(n-1)\cdot\gamma}{\gamma_{min}}\right) \qquad (12)$$

The best-fit parameters summarised in Table 1 were used to represent the sludge rheology and integrated in our CFD model.

The CFD model was validated using experimental data from a lab-scale digester [29], and the model setup was consistent with the optimisation achieved in our previous model [9]. Fig. 3A shows the local axial velocity distributions, including both the Ostwald and Herschel-Bulkley (35 °C) cases and the measured data [29]. In our previous work [9], a good agreement was achieved by a critical model validation (Ostwald ref. in Fig. 3A), and considerable rheological impacts on the flow prediction were found. Because the studied sludge was much more viscous than the sludge in our previous work, the induced sludge flows were more constrained, leading to shrunk velocity profiles inside the draft tube ($r/R < 0.2$) and little flow-loop outside the draft tube ($r/R > 0.2$, height 18.25 cm). So, differences in the velocity profiles were expected, and a reasonable agreement was obtained.

Fig. 3A shows relatively small velocity differences between the Ostwald and Herschel-Bulkley model predictions. However, the differences in mixing performance were much larger. As shown in Fig. 3B, the Herschel-Bulkley case had much longer time to reach good (90%) and ideal (95%) mixing (over 2 and 1.5 times, respectively) than Ostwald, indicating considerable impacts of the rheological differences at low shear rates that could not be fully revealed in the velocity data.

3.2. Flow and mixing characterisation: Ostwald vs. Herschel-Bulkley

3.2.1. Ostwald: Model applicability and limitation

The impacts of the rheological differences at low shear rates on flow and mixing were further investigated in the studied full-scale digester. For the Ostwald model, the change in μ becomes quite large at low shear rates within the effective range. A sensitivity study on the effective range limit was carried out, which was described in Supplementary B. The results showed considerable differences in flow and mixing predictions when there were small changes in γ_{min} (correlated with μ_{max}). To minimise this range limit effect on the results, the largest effective range (γ 1–300 s^{-1}) determined with satisfactory fitting performance was applied in the subsequent simulations.

Flow and mixing behaviour of the Ostwald model is shown in Fig. SC-1 (Supplementary C) using a cross section containing two gas lances. Generally, gas phase distributions and induced sludge flows were mainly constrained in regions close to the gas lances; vertical-dominant flow
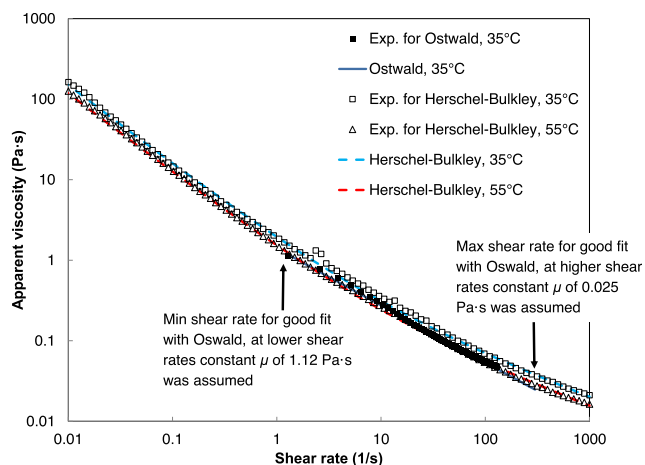

Fig. 2. Sludge rheological data, experimental (averaged standard deviation in each curve $\leq 5\%$) and model fitting by Ostwald and Herschel-Bulkley models.

Table 1
Sludge rheological parameters fitted by Ostwald and Herschel-Bulkley models, based on the best fitting performance using the sum of squared errors and the root mean squared error.

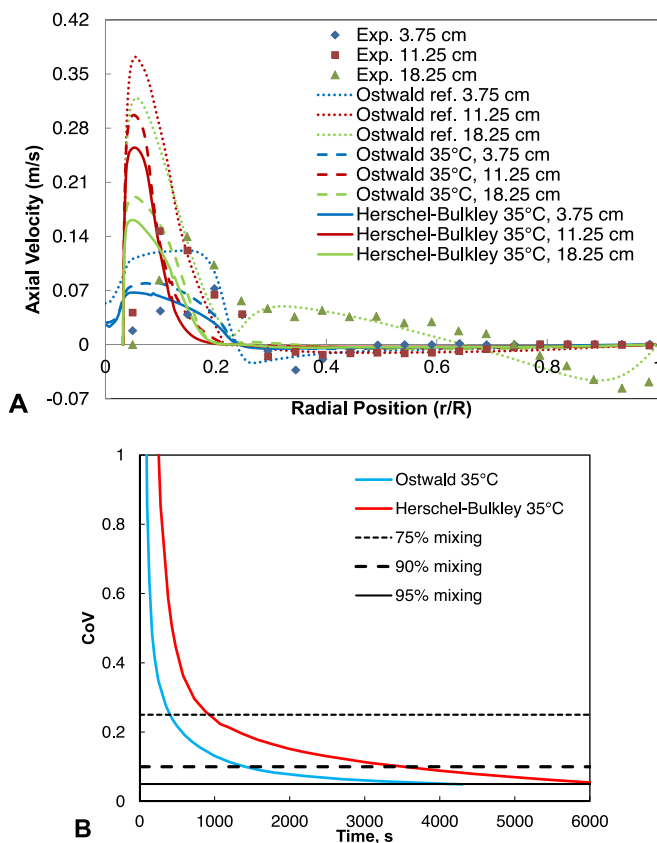|	Rheological properties		
	K, Pa·s^n	n, -	τ_0, Pa
Ostwald, 35 °C	1.40	0.292	–
Herschel-Bulkley, 35 °C	0.49	0.526	1.45
Herschel-Bulkley, 55 °C	0.39	0.525	1.15

Fig. 3. Flow and mixing results of the lab-scale model (gas flow rate 56.64 L/h) for validation, (A) local axial velocity distributions, with the referred experimental [29] and our previous validated CFD [9] data; (B) CoV curves.

behaviour was obtained in the tank, with poor-flow regions below the gas inlet. This plug-flow pattern was clearly reflected in the mixing performance (Fig. SC-1D). Tracer mass transfer was dominated by convection in accordance with the vertical flows, while dispersion by the horizontal flows and turbulence was weak. More flow and mixing details of Ostwald, 35 °C are described in Supplementary C. Because the localised plug-flow behaviour was similar to our lab-scale results (Section 3.1 and [9]), similar mixing problems can be expected in a scaled-up process of gas-mixed digesters.

As shown in Fig. 4A, the major part of the domain was covered by sludge velocities in a range < 0.1 m/s, and the low velocity level (< 0.01 m/s) was mainly distributed near the bottom of the digester. The considerable velocity heterogeneity also correlated to the mixing performance assessed by the tracer's CoV data. As shown in Fig. 4B, the CoV curve had a varying deceasing tendency, with an exponential decay when approaching to the ideal (95%) mixing degree. As discussed in Supplementary B, the CoV results indicated that the medium and high velocity levels (> 0.01 m/s) above the gas inlet mainly accounted for reaching a medium mixing degree (75%). However, for reaching a higher mixing degree (over 90%), the relatively small volume fraction of the low velocity level became more important, which directly correlated to the apparent dead-zone in the digester.

It should be noted that different dead-zone definitions have been employed in previous studies [4,17,29–31]. In some studies, the dead-zone is defined by velocities below 5% of the maximum velocity (v_{max}) [4,17,31]. However, this definition relies on flow field stability, and seems not effective when strong v_{max} fluctuations are observed in the digester [11]. Although our results showed small v_{max} fluctuations, the highest velocity level (> 1 m/s) was mainly located in the constrained regions near the gas lances; the volume fraction was too small ($< 0.2\%$) to represent or affect the dominant velocity. Hence, the

definition was not appropriate to be applied in this study. Besides, the dead-zone can be determined by Stokes' settling velocity ($v_{settling}$), which is calculated by [32]

$$v_{settling} = \frac{\rho_p - \rho_l}{18 \cdot \mu_l} \cdot g \cdot d_p^2 \tag{13}$$

where d_p denotes the particle diameter. This dead-zone definition has also been applied in some studies, and the $v_{settling}$ specific to the referred biomass (diameter 250 μm and density 1050 kg/m^3) is in the order of 10^{-3} m/s [29,30]. However, the estimation is based on a μ_l magnitude comparable to water viscosity, and thus needs to be adapted in our sludge scenario. Referring to biomass with similar characteristics, the highest $v_{settling}$ determined by μ_{min} (0.025 Pa•s) was in a much lower order of 10^{-5} m/s in this study, resulting in almost no dead-zone predictions. It has been reported that the characteristic sludge-particle sizes in digesters are usually smaller than 250 μm [33,34], and the sludge density does not change much to the solids content [15]. So, any further changes in the biomass density and particle size would not result in much higher $v_{settling}$, indicating inappropriate dead-zone determination for the studied sludge. Nevertheless, this definition could still be useful in interpreting the sand/gravel sedimentation observed in the studied digester. Regarding fine gravel (density 2650 kg/m^3) with 5 mm particle diameter, the dead-zone determined by $v_{settling}$ presented a large volume fraction of 40%. Hence, the applied gas-sparging strategy could moderately maintain the sludge matrix in suspension, but seems not enough to prevent accumulative sedimentation of other contained denser materials (such as fine gravel), which could lead to a considerable reduction in effective volume during long-term operation (observed in reality).

Moreover, the Ostwald model results revealed an important role of the effective range in flow and mixing predictions, which could limit model applications. The Ostwald model generally fits well at medium and high shear rates, so the determined γ_{min} is usually not low. As shown in Table 2, γ_{min} of 11 s^{-1} has been determined for fitting the experimental rheological data [18,19], and has been referred to in many CFD modelling studies [3,7,12,15–17]. However, the values for γ in full-scale anaerobic digesters are only reported in one study, with average γ values around 0.2 s^{-1} [12]. This magnitude is smaller than the referred γ_{min}, but the difference has not been further discussed. A comparable volume-average γ value of 0.14 s^{-1} was obtained in this study, which was also smaller than the applied γ_{min} of 1 s^{-1}, and much smaller than the γ_{min} of 11 s^{-1} in literature shown in Table 2. In addition, considerable γ gradients were observed in the whole domain, with low γ (< 1 s^{-1}) in large space (Fig. 4C). As discussed in Supplementary B, the dominant γ was out of the effective range, leading to an 'almost Newtonian fluid' prediction with constant μ_{max} in most regions.

According to the authors' knowledge, the impact of the rheological effective range on flow and mixing characterisation has not been investigated thus far. But its importance, especially on γ_{min}/μ_{max} determination, was clearly revealed in our results. The Ostwald model should be carefully applied to assess sludge flow and mixing. If the dominant γ in an installation is in the determined effective range, the Ostwald model can be a better option than the other rheological models because of its lower complexity. However, regarding the γ results obtained in this study and the reference [12], the dominant γ in real full-scale gas-mixed digesters could be expected in the same order of 0.1 s^{-1}, out of the model's range. Hence, the Ostwald model application can result in underestimation of the overall μ magnitude, and thus overestimation of the flow and mixing performance. To address the challenge that the shear rate of sludge flows in practice are uncoupled with the model fitting range, improved rheological characterisation of digester sludge, including experimental measurements and data fitting, is recommended, which should be extended to the low shear rates.
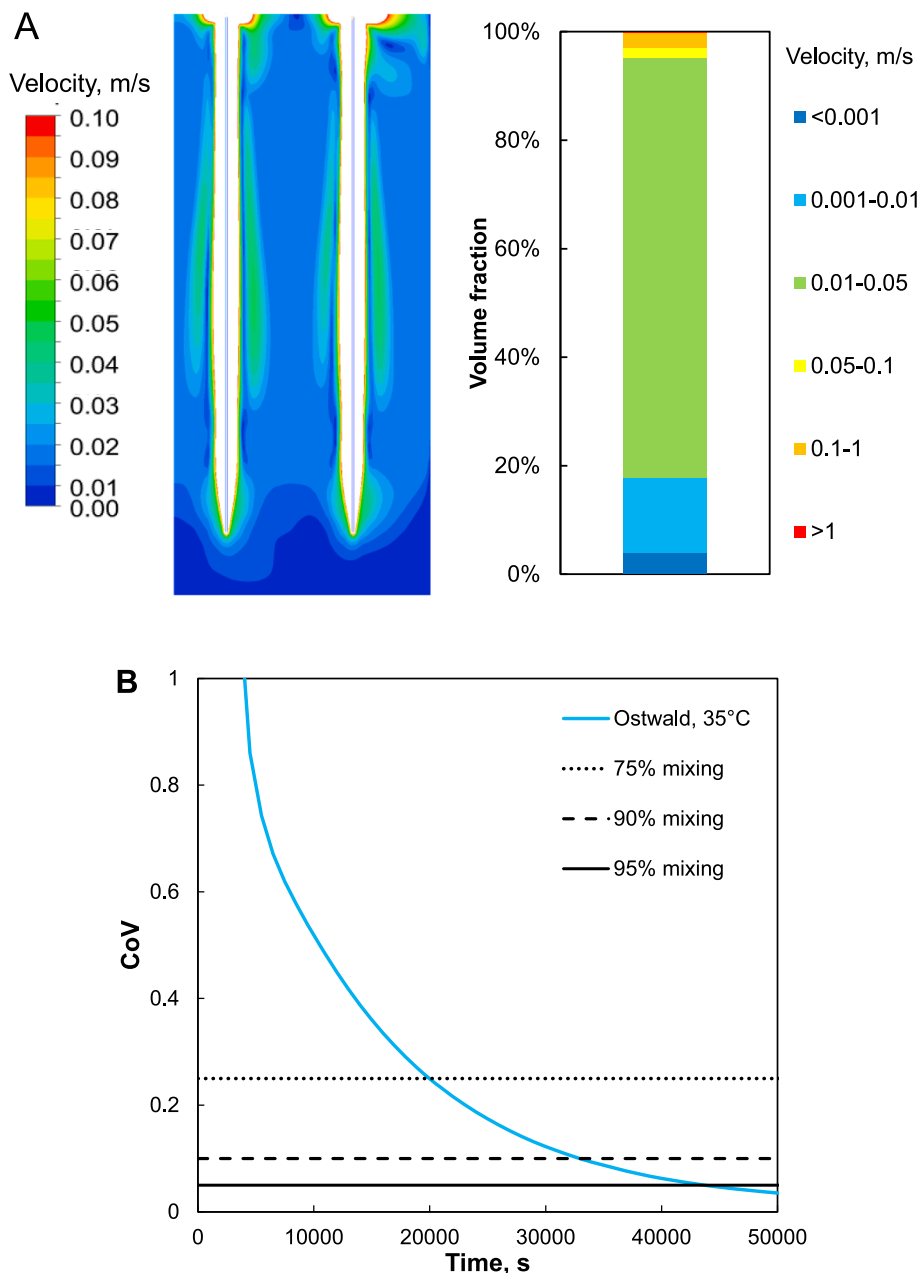
Fig. 4. Flow and mixing behaviour of Ostwald, 35 °C: (A) sludge velocity contour (left) and volume fraction distribution (right); (B) CoV curve; (C) shear rate contour (left) and volume fraction distribution (right).

3.2.2. Herschel-Bulkley: Improvements at low shear rates

Compared to the Ostwald model, the Herschel-Bulkley model has an enlarged effective shear rate range from 0.01 to 1000 s^{-1} (Table 2), so a much larger μ was obtained at low shear rates ($\gamma < 1$ s^{-1}). As shown in Fig. 5A and 5B, Herschel-Bulkley, 35 °C obtained large volume fractions with velocities < 0.5 m/s and $\gamma < 0.1$ s^{-1} (57% and 68%, respectively).

Fig. 5C shows viscosity contours of the two models, in which a 15 mm bubble size was used (discussion on bubble size is addressed in Section 3.3.2). Effective viscosity (μ_{eff}) was applied to involve a turbulence impact, which is the sum of the sludge apparent viscosity (μ) and turbulent viscosity (μ_{turb})

$$\mu_{\text{eff}} = \mu + \mu_{\text{turb}} \tag{14}$$

The two models showed distinct μ_{eff} distributions in the domain. For the Ostwald model, the volume-average μ was close to μ_{max} (1.12 Pa•s), so μ_{turb} (volume-average 26.6 Pa•s) was the dominant component in μ_{eff}. As shown in Fig. 5C (Ostwald, 35 °C), high μ_{eff} (with μ_{turb} being dominant) was found above the gas inlet, especially in regions between the gas lances. However, the Herschel-Bulkley model (35 °C) demonstrated opposite results: the volume-average μ of 69.5 Pa•s was much larger than μ_{turb} (volume-average 3.9 Pa•s), and became dominant in μ_{eff}. As shown in Fig. 5C (Herschel-Bulkley, 35 °C), the high μ_{eff} distribution between the gas lances could be mainly ascribed to μ rather than to μ_{turb}. Moreover, much larger μ_{eff} gradients were obtained and high values of μ_{eff} were mainly found below the gas inlets. It should be noted that turbulence modelling by the RANS method in non-Newtonian flows is still challenging, because the viscosity term in the momentum equation is no longer constant but correlated with the shear rate. This term highly
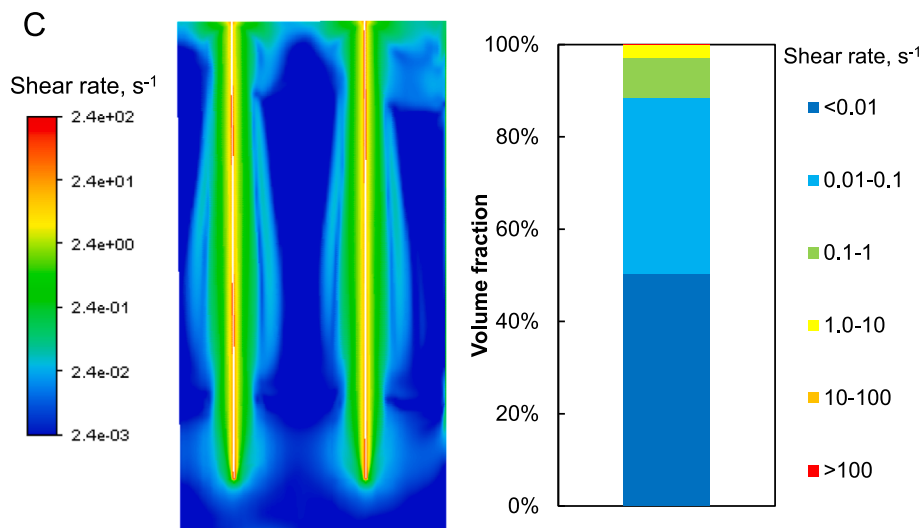
Fig. 4. (*continued*).

Table 2

Ranges of shear rate (γ) and apparent viscosity (μ) in different datasets.

	Ostwald		Herschel-Bulkley	
	γ, s^{-1}	μ, Pa·s	γ, s^{-1}	μ, Pa·s
Determined by data fitting	1–300	0.025–1.12	0.01–1000	0.02–162
Predicted by the used CFD model	−236*	0.029–1.12	−1007*	0.02–297
Applied in references [3,7,12,15–17]	11–702	0.006–0.17	0.01–30	0.02–13.3

*with very small γ_{min} ($< 10^{-4}$ s^{-1}).

depends on the stress-deformation relation that is expressed as the rheological models [35]. Presumably an additional non-Newtonian Reynolds stress tensor may need to be solved [36], understanding of which is still unclear [36,37]. Solving this fundamental challenge is beyond the scope of our research. So, any in-depth discussion on turbulence, regarding its localised and constrained distribution, is not further addressed.

Similar to the μ_{eff} distributions, distinct mixing behaviour between the two models was also observed. Statistical analysis on local tracer concentrations (i.e., changes in c_i - c_m in Equation (11) in some key locations) was also carried out to comprehensively assess the mixing performance. Fig. 6A shows variation of the area-average tracer concentration at two heights: 1.5 m (just below the gas inlet), and 0.1 m (near the bottom). Here, dimensionless mixing time θ was used, normalised by the ideal mixing time:

$$\theta = \frac{t}{t_{95\% \ mixing}} \tag{15}$$

The two Ostwald 35 °C curves (1.5 m and bottom) showed a similar tendency: the lag of the tracer dispersion from 1.5 m to the bottom was low, i.e., $\theta \sim 0.03$, and the concentration difference became negligible when $\theta > 0.5$. However, the two Herschel-Bulkley 35 °C curves showed distinct tendencies. The 1.5 m curve yielded shorter θ for the first appearance of the tracer, and then had a steep and monotonic increase to a plateau. The bottom curve yielded a lag θ similar to the Ostwald model, but then had a much slower increase. When reaching the ideal mixing (θ = 1), the concentration difference between the two curves was still not negligible. Hence, the Herschel-Bulkley model revealed a different tracer dispersion pattern, indicating considerable segregation. The highly heterogeneous μ_{eff} distribution accounted for the segregation: the tracer transfer from top to the gas inlet height was fast; but further

penetration to the bottom became much slower. These localised differences were further reflected in the overall mixing performance. As shown in Fig. 6B, considerable differences were observed after reaching the 75% mixing degree between Ostwald and Herschel-Bulkley (35 °C). Like Fig. 4B, the Ostwald curve had an exponential decay. However, the Herschel-Bulkley curve had a power-law decay, indicating much more time to reach the ideal mixing degree. Accordingly, $t_{95\% \ mixing}$ values of Ostwald and Herschel-Bulkley had an order of magnitude difference, which were 3×10^3 s and 7×10^4 s, respectively.

The considerable discrepancy in flow and mixing predictions further revealed the intrinsic limitation of the Ostwald model. The simplified μ assumption at low shear rates led to the absence of the segregation prediction, and thus to considerable flow and mixing performance overestimation. This limitation was negated using the Herschel-Bulkley model, due to more accurate descriptions of the highly sensitive μ changes at low shear rates. Therefore, the Herschel-Bulkley model was used in the following simulations. In addition, the predicted segregation pattern directly correlated to poor mixing performance, and thus was more meaningful to determine the dead-zone than the several definitions discussed in Section 3.2.1.

3.2.3. Mesophilic vs. thermophilic: The rheological impact

The aforementioned simulations were based on the mesophilic digestion conditions operated at 35 °C. Anaerobic digestion is also commonly implemented at thermophilic conditions, applying a temperature of 55 °C [38,39]. As reported in our previous study [21], the studied sludge had a systematic 20% decrease in μ when increasing the temperature from 35 °C to 55 °C (also shown in Fig. 2). Accordingly, potential changes in resulting flow and mixing under thermophilic temperature conditions were assessed. As shown in Figs. 5 and 6, the Herschel-Bulkley 55 °C case had higher velocity and shear rate than Herschel-Bulkley 35 °C, with a volume fraction decrease of 22% in velocity < 0.5 m/s, and 16% in $\gamma < 0.1$ s^{-1}. The volume-average μ_{eff} had a substantial decrease of 49% to 37.2 Pa·s, but μ (volume-average 30 Pa·s) was still dominant, and the μ_{eff} gradients were still large. These results indicated considerable segregation as well, which was clearly reflected by the mixing performance at local heights (Fig. 6A) and the whole domain (Fig. 6B), like Herschel-Bulkley 35 °C. The 55 °C CoV curve also had a power-law decay after reaching the 75% mixing degree. Nonetheless, the time scale was much smaller, with a 59% decrease in the ideal mixing time to 2.8×10^4 s.

Compared to the mesophilic mode, the thermophilic mode has been reported to offer various advantages, including higher conversion rate of
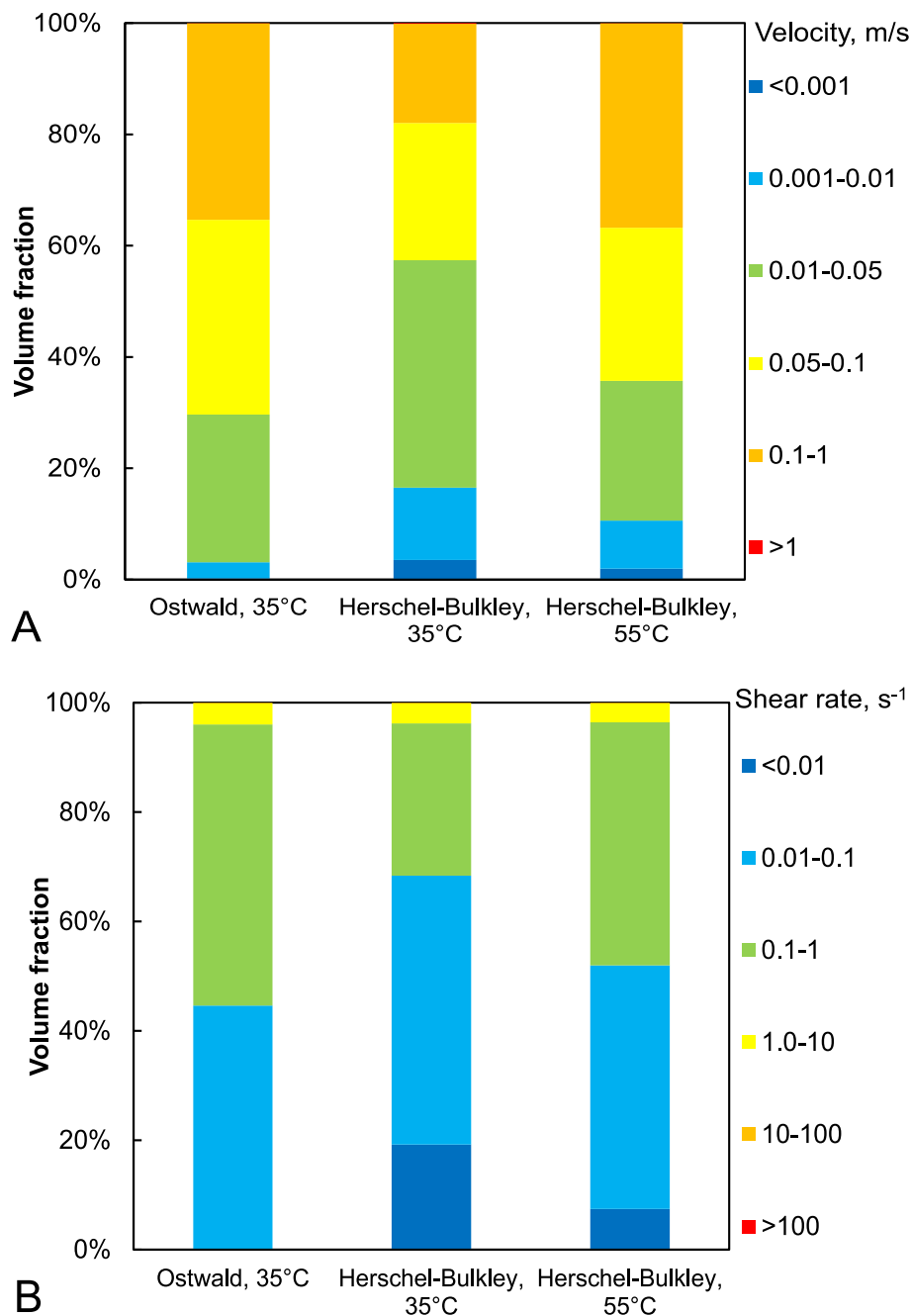
Fig. 5. Flow behaviour of the Ostwald and Herschel-Bulkley models: volume fraction distributions of (A) velocity; (B) shear rate; (C) contours of effective viscosity.

organic solids, improved dewatering characteristics and higher die-off of pathogenic organisms [38,39]. In this study more advantages were revealed: better flow and mixing performance resulting from lower μ of the sludge matrix, and thus a better use of the whole effective volume. If the benefit from the improved operational performance compensates the extra energy required for the higher working temperature, thermophilic digestion could be an alternative for optimisation of the studied digester.

3.3. Gas-sparging for mixing: Assessment and guidelines for optimisation

3.3.1. Flow and mixing enhancement by gas-sparging

The flow and mixing performance was further assessed using more tracer data at local heights. In addition to 1.5 m and the bottom, three heights above the gas inlet were included, which were nearly 1/3 (5 m),

2/3 (10 m), and the whole height (15 m) of the digester, respectively. As shown in Fig. 6C (Herschel-Bulkley 35 °C), the curves at the three heights had more fluctuations before being stabilised, which was different from the plateau tendency in the 1.5 m curve. These differences indicated distinct tracer dispersion patterns referring to the gas inlet height (1.75 m). Above the gas inlet, the tracer dispersion displayed a plug-flow pattern mainly affected by the vertically-dominant flows. After being released from the top, the concentrated tracer bulk moved towards the bottom first, and its motion at each height was tracked by the first peak in the curve. Based on the peak time lag, a characteristic vertical dispersion rate of 0.06 m/s was estimated. Below the gas inlet, the tracer dispersion to the bottom had a monotonic penetration pattern due to the considerable segregation, and had a much lower rate of 0.2 mm/s. Therefore, two clearly distinguishable compartments with
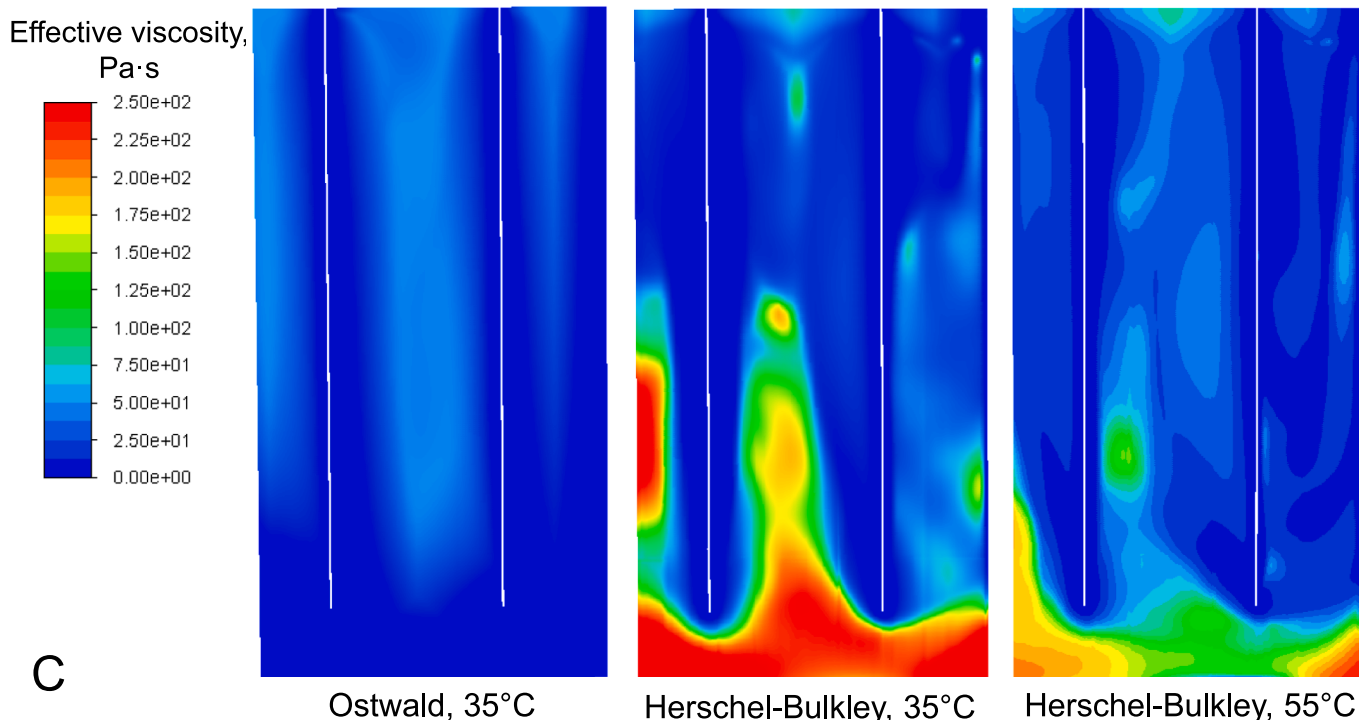
Fig. 5. (*continued*).

distinct flow and mixing behaviour were obtained based on the gas inlet location: a plug-flow compartment above, and a dead-zone compartment below.

In addition, several representative flow and mixing time scales were estimated based on the curves in Fig. 6C. An effective vertical dispersion through the domain bulk (above 1.5 m) had a time scale up to 600 s. An effective horizontal dispersion had a time scale of about 2000 s, whereas negligible differences were obtained in the tracer concentration across all heights above 1.5 m. Therefore, the applied gas-sparging operation was supposed to enhance flow and mixing with: 1) a fast vertical dispersion in an order of 10^2 s ($<$ 10 min); 2) a slower centre-side dispersion rate in the order of 10^3 s ($>$ 20 min); and 3) a much lower ideal mixing in the order of 10^4 s ($>$ 3 h). These time scales should be seen in relation to the mean residence time in the digester of 27 days.

Although the insufficient mixing and resulting flow created a considerable gap with the ideal CSTR expectation, the applied gas-sparging operation could still be crucial for the operation of the studied digester. Regarding the layout (Fig. 1A), the location difference between the sludge feed point (4.25 m height) and the discharge point (16 m height, opposite side of the feed point) could easily result in short-circuiting, if no gas-sparging were applied. As shown in Fig. 7A, the gas-sparging by the 21 gas lances created considerable vertical-dominant convection through the digester. Thus, it could moderately maintain the effective volume and mitigate the short-circuiting, which is important for attaining the long-term digestion performance. However, the considerable segregation in the dead-zone compartment was a critical shortcoming and should be solved by improving the gas-sparging performance. Furthermore, Fig. 7 shows different flow patterns between two sludge sources, and a much better flow performance (Fig. 7B) was estimated using the referred sludge [18,19]. Our results reveal another limitation that was not further explored in the previous studies [3,7,12,15–17]: if the rheological data integration does not match with the sludge source treated in the installation, there is a risk of incorrect assessment on flow and mixing performance.

It should be noted that our present work does not include the randomly produced biogas bubbles in the digestion process itself. In the studied digester, an average biogas production of 2450 m^3/day is obtained (full-scale data, not shown), which is randomly released, resulting in bubbles of different sizes. Very likely, also the laminar and turbulent flows brought about by these biogas bubbles contribute to the mixing and prevention of short circuiting between the sludge feed point and discharge point.

3.3.2. Guidelines for optimisation and design in practice

Some guidelines for process optimisation at full scale can be proposed based on the results of this study.

(1) Gas-sparging intensity.

Gas-sparging intensity determines the amount of injected biogas for mixing and is consequently an important operational parameter to assess. Based on the compressor's capacity, the injected biogas flow rate was calculated to be 300 m^3/h in the studied digester. Two more biogas flow rates were considered, i.e., 150 and 450 m^3/h, which agree with a respective 50% decrease and 50% increase of the reference of 300 m^3/h. As shown in Table 3 (row 1–3), the overall mixing performance was improved when increasing the biogas flow rate, although some trends were not monotonic due to the dynamic flow field. However, the flow and mixing enhancement was insufficient, considering the applied large increase in biogas flow rate (a factor 3, from 150 to 450 m^3/h), and, therefore, likely not of much practical use. Energy consumption for the gas-sparging was evaluated based on the power input calculation [40]

$$E = P_1 \cdot Q \cdot ln\left(\frac{P_2}{P_1}\right) \qquad (16)$$

where Q denotes the gas flow rate; and P_1 and P_2 are the absolute pressure in the tank headspace (1 atm) and at the gas-sparging inlet (3 atm), respectively. The mixing energy level (*MEL*) can be estimated following [41]

$$MEL = \frac{E}{V} \qquad (17)$$

where V denotes the effective volume of the digester. The realistic 300 m^3/h scenario yielded a *MEL* of 2.1 W/m^3, which was close to 2.2 W/m^3
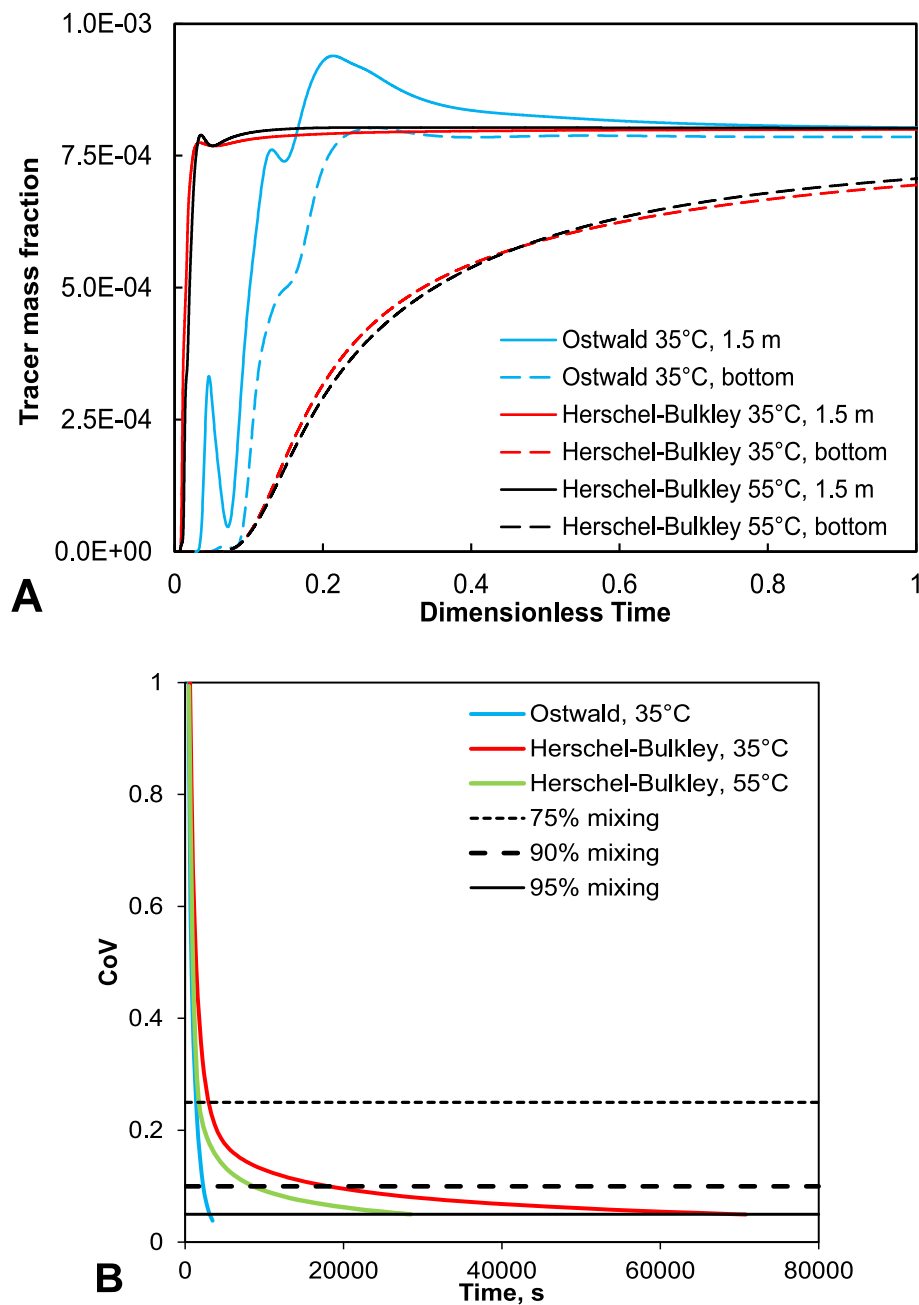
Fig. 6. Mixing behaviour of the Ostwald and Herschel-Bulkley models, (A) area-average tracer concentration at local heights; (B) CoV in the whole domain; (C) area-average tracer concentration at different heights, Herschel-Bulkley, 35 °C.

reported in another full-scale gas-mixed digester [12]. Mixing was improved in the 450 m³/h scenario, but the increased *MEL* (3.2 W/m³) was still much lower than the recommended range of 5–8 W/m³ for proper mixing [42]. To match the recommended range, the current compressor capacity should be increased by at least a factor 2.4 to over 710 m³/h. Such change requires more investment, more technical adjustment and much larger energy consumption, which may challenge the net energy benefit, not being attractive for the studied digester. Therefore, intensifying the gas-sparging rate seems not an efficient strategy to enhance flow and mixing, and the recommended *MEL* criterion appears unsuitable for the studied digester.

(2) Bubble size.

As a further step to our lab-scale study [9], the impact of bubble size on flow and mixing in the full-scale digester was assessed. Compared to lab-scale, bubble size distribution is expected to be more complicated in the full-scale scenario, due to the large dimension (16 m height), the different gas-sparging equipment and uncertain size changes from bubble coalescence or break-up. However, no experimental data on bubble size have been obtained in the studied digester. Thus, necessary simplifications were made, and a uniform bubble size was assumed. A size of 5 mm was set based on our lab-scale model [9], but larger sizes up to 30 mm were considered due to the quite large hydrostatic pressure change (over 1.5 atm) and large diameter of the gas lances. As shown in Supplementary D (Fig. SD-1A), the bubble size had a considerable effect on the sludge velocity distributions. In particular, the volume fraction of velocity > 0.05 m/s showed a large increase when the bubble size increased to over 15 mm. The mixing performance results are also included in Table 3 (row 2, and 4–6). Due to the increased overall
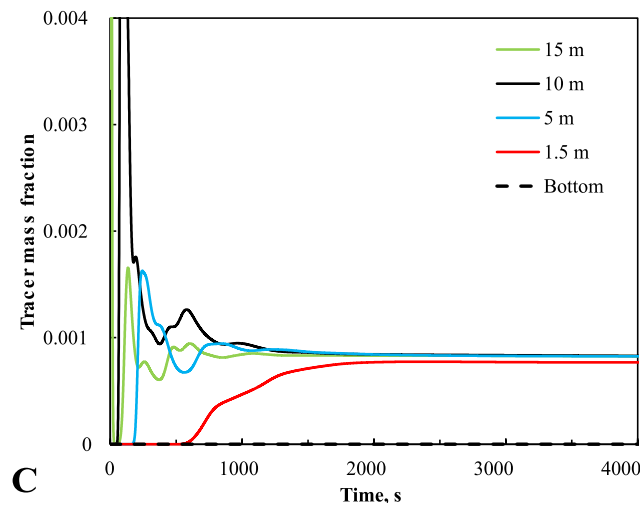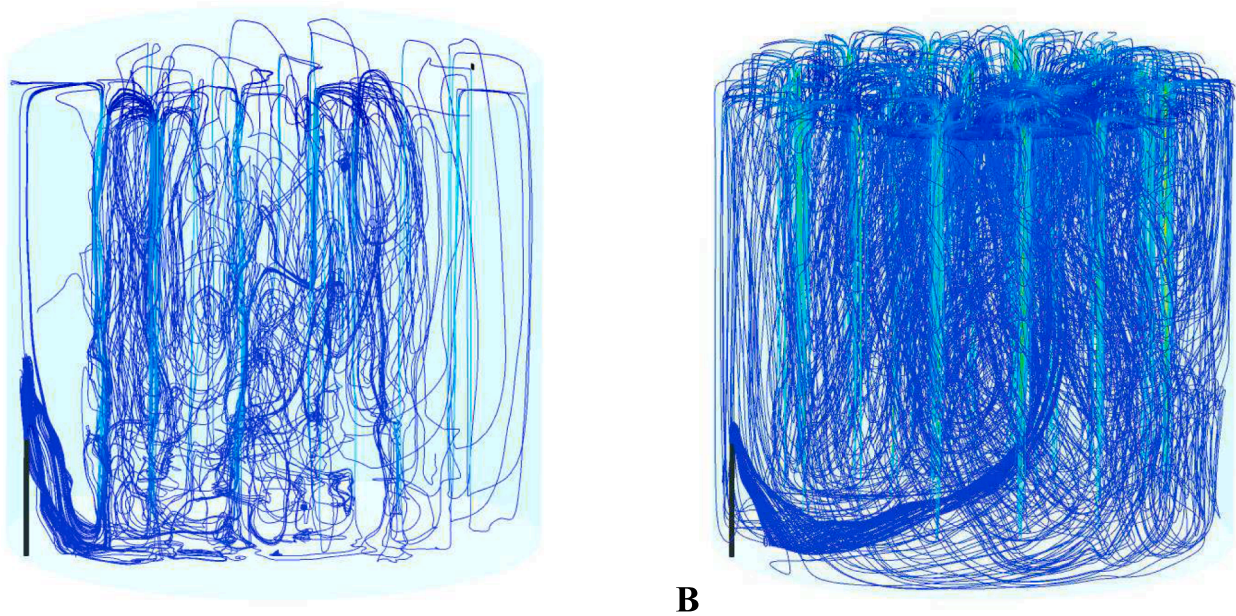
Fig. 6. (*continued*).

Fig. 7. Schematic streamlines (starting from the sludge feed location) in the whole digester filled with different sludge sources, (A) the locally treated sewage sludge; and (B) referred manure slurry [18,19].

Table 3
Mixing time data of different scenarios. The specified mixing degree in % was determined by the CoV data, as described in Section 2.2.3.

Variable		Mixing time, $\times 10^3$ s			
		50%	75%	90%	95% (ideal)
Gas-sparging rate (bubble size 5 mm)	150 m³/h	0.62	3.44	25.42	107.22
	300 m³/h	0.65	5.17	25.85	62.27
	450 m³/h	0.40	3.26	18.94	56.91
Bubble size (gas-sparging rate 300 m³/h)	10 mm	0.76	3.08	25.97	64.68
	15 mm	0.96	2.38	16.91	68.15
	30 mm	0.51	1.61	15.98	73.18
Gas inlet height 0.5 m (300 m³/h, bubble size 15 mm)		0.78	1.14	3.82	13.75

velocity magnitude when applying larger bubbles, the moderate and good mixing degrees (up to 90%) were reached faster, indicating improved mixing performance in the plug-flow compartment. However, larger bubbles could not move below the gas inlet to considerably reduce the space of the dead-zone compartment, so the ideal mixing performance did not change much with the increased bubble size.

The 15 mm bubble size scenario, represents a moderate bubble size and induces moderate flow and mixing performance, and was thus applied most in this study. It should be noted that the simplifications in the bubble size setup were a necessary trade-off between simulation accuracy and feasibility. Therefore, it remains questionable if the realistic biogas flow and mixing performance has a good quantitative agreement with any bubble size scenario. However, the predicted qualitative tendencies of flow and mixing were important, because larger bubbles accounted for stronger phase interactions and thus stronger disturbance in sludge flows. Compared to increased gas-sparging rate, larger bubbles can achieve comparable mixing enhancement but do not require more power input from the compressor, and

thus can be more applicable in practical optimisation. The applied gas lances are basically long open tubes allowing only limited size control of released bubbles. A layout modification or a new design of the gas lances could be an option for generating larger bubbles. In addition, biogas production from sludge digestion creates bubbles with varying sizes in the digester. Owing to sludge rheology (yield stress) these bubbles may reach very large dimensions, causing biogas eruptions from the sludge, particularly when the sludge is not well mixed. While escaping from the liquid stagnant zone, these bubbles likely cause regions of turbulence, which are not considered in our current work. Future work to consider the impact of the generated biogas bubbles on flow and mixing will be highly valuable.

(3) Height of the gas inlet.

As discussed in Section 3.3.1, the gas inlet location largely determined the two-compartment pattern. To mitigate the segregation in the dead-zone compartment, a lower gas inlet height of 0.5 m was considered. Fig. SD-1B shows the γ distributions (mesophilic). Compared to 1.75 m, the 0.5 m scenario yielded a considerable fraction decrease (from 19.2% to 6.4%) in $\gamma < 0.01$ s^{-1}, and the volume-average μ_{eff} reduced by 41% to 43.4 Pa•s. As shown in Table 3, the time to reach good mixing degrees also largely decreased. Similar changes in flow and mixing were obtained in the thermophilic 0.5 m scenario (data not shown).

With the low gas inlet height, the gas-sparging operation activated more sludge motion close to the bottom. The overall velocity and shear rate increased considerably (15% and 17%, respectively), resulting in a reduced volume of the dead-zone compartment. Moreover, the low gas inlet height helps to further mitigate short-circuiting, sedimentation and to maintain the effective volume in long-term operation. Compared to the thermophilic alternative as discussed in Section 3.2.3, the lower gas inlet height did not reduce the μ but still considerably enhanced the flow and mixing performance. Regarding practical optimisation, it is more feasible to change the gas inlet height than the operational temperature in an existing digester, yet more attention should be paid to higher energy costs for gas-sparging from a deeper location, and potential blockages, i.e., with accumulating sand/gravel, as observed in the studied digester.

The authors are aware of the limited validation of the modelling approach that was used for this specific application, which is ascribed to the inaccessibility of a full-scale reactor for measuring flow regimes and mixing processes. However, the sensitivity analysis performed in this study revealed the consequences of modifications to the viscosity model and the required changes for reactor operation in a qualitative way. To the author's understanding, the latter justifies the further exploration of optimising the conversion processes in practice.

4. Conclusions

The model, which was firstly validated using a lab-scale setup, showed that flow and mixing characterisation considerably depended on the sludge rheological data input in a full-scale digester. The predicted dominant shear rate in the digester was out of the effective shear-rate range of the Ostwald model, leading to flow and mixing performance overestimation. The results indicated that the Ostwald model and the conventional approaches used to determine dead-zones have limitations.

However, the Herschel-Bulkley model was more appropriate for the prevailing low shear rates and predicted large viscosity gradients in the digester. The results revealed distinct flow and mixing compartments determined by the gas-sparging height: a plug-flow compartment with dominant vertical convection above, and a dead-zone compartment with considerable segregation below. Time scales to reach medium and ideal mixing had orders of magnitude differences. Although inducing insufficient flow and mixing, the applied gas-sparging still contributed to prevent short-circuiting, accumulative sedimentation and effective volume reduction. To correctly assess flow and mixing, the applied

rheological data should be in agreement with the type of sludge that is treated in the digester.

Overall, the shear rate in the digester should be increased, which, however, cannot be efficiently achieved by simply intensifying the gas-sparging rate. It is recommended to reduce the gas-sparging height, or to enlarge the overall bubble size. Thermophilic operation under reduced sludge viscosity could also be an alternative, provided that the improved operational performance compensates the additional energy requirement.

Declaration of Competing Interest

The authors declare that they have no known competing financial interests or personal relationships that could have appeared to influence the work reported in this paper.

Data availability

Data will be made available on request.

Appendix A. Supplementary data

Supplementary data to this article can be found online at https://doi.org/10.1016/j.cej.2023.143647.

References

[1] J. Lindmark, E. Thorin, R. Bel Fdhila, E. Dahlquist, Effects of mixing on the result of anaerobic digestion: Review, Renew. Sustain. Energy Rev. 40 (2014) 1030–1047.

[2] I. Capela, M.J. Bilé, F. Silva, H. Nadais, A. Prates, L. Arroja, Hydrodynamic behaviour of a full-scale anaerobic contact reactor using residence time distribution technique, J. Chem. Technol. Biotechnol. 84 (2009) 716–724.

[3] M. Terashima, R. Goel, K. Komatsu, H. Yasui, H. Takahashi, Y.Y. Li, T. Noike, CFD simulation of mixing in anaerobic digesters, Bioresour. Technol. 100 (2009) 2228–2233.

[4] M.S. Vesvikar, M. Al-Dahhan, Flow pattern visualization in a mimic anaerobic digester using CFD, Biotechnol. Bioeng. 89 (2005) 719–732.

[5] K. Karim, G.J. Thoma, M.H. Al-Dahhan, Gas-lift digester configuration effects on mixing effectiveness, Water Res. 41 (2007) 3051–3060.

[6] A.R. Coughtrie, D.J. Borman, P.A. Sleigh, Effects of turbulence modelling on prediction of flow characteristics in a bench-scale anaerobic gas-lift digester, Bioresour. Technol. 138 (2013) 297–306.

[7] D. Dapelo, F. Alberini, J. Bridgeman, Euler-Lagrange CFD modelling of unconfined gas mixing in anaerobic digestion, Water Res. 85 (2015) 497–511.

[8] B. Sajjadi, A.A.A. Raman, R. Parthasarathy, Fluid dynamic analysis of non-Newtonian flow behavior of municipal sludge simulant in anaerobic digesters using submerged, recirculating jets, Chem. Eng. J. 298 (2016) 259–270.

[9] P. Wei, R.F. Mudde, W. Uijttewaal, H. Spanjers, J.B. van Lier, M. de Kreuk, Characterising the two-phase flow and mixing performance in a gas-mixed anaerobic digester: Importance for scaled-up applications, Water Res. 149 (2019) 86–97.

[10] B.X. Wu, CFD simulation of gas and non-Newtonian fluid two-phase flow in anaerobic digesters, Water Res. 44 (2010) 3861–3874.

[11] D. Dapelo, J. Bridgeman, Assessment of mixing quality in full-scale, biogas-mixed anaerobic digestion using CFD, Bioresour. Technol. 265 (2018) 480–489.

[12] D. Dapelo, J. Bridgeman, Euler-Lagrange Computational Fluid Dynamics simulation of a full-scale unconfined anaerobic digester for wastewater sludge treatment, Adv. Eng. Softw. 117 (2018) 153–169.

[13] N. Eshtiaghi, F. Markis, S.D. Yap, J.-C. Baudez, P. Slatter, Rheological characterisation of municipal sludge: A review, Water Res. 47 (2013) 5493–5510.

[14] I.D. Kariyama, X. Zhai, B. Wu, Influence of mixing on anaerobic digestion efficiency in stirred tank digesters: A review, Water Res. 143 (2018) 503–517.

[15] B.X. Wu, S.L. Chen, CFD simulation of non-Newtonian fluid flow in anaerobic digesters, Biotechnol. Bioeng. 99 (2008) 700–711.

[16] B.X. Wu, Computational Fluid Dynamics investigation of turbulence models for non-Newtonian fluid flow in anaerobic digesters, Environ. Sci. Tech. 44 (2010) 8989–8995.

[17] J. Bridgeman, Computational fluid dynamics modelling of sewage sludge mixing in an anaerobic digester, Adv. Eng. Softw. 44 (2012) 54–62.

[18] A. Achkari-Begdouri, P.R. Goodrich, Rheological properties of Moroccan dairy cattle manure, Bioresour. Technol. 40 (1992) 149–156.

[19] H. Landry, C. Laguë, M. Roberge, Physical and rheological properties of manure products, Appl. Eng. Agric. 20 (2004) 277–288.

[20] P. Wei, Q. Tan, W. Uijttewaal, J.B. van Lier, M. de Kreuk, Experimental and mathematical characterisation of the rheological instability of concentrated waste activated sludge subject to anaerobic digestion, Chem. Eng. J. 349 (2018) 318–326.

[21] P. Wei, W. Uijttewaal, J.B. van Lier, M. de Kreuk, Impacts of shearing and temperature on sewage sludge: Rheological characterisation and integration to flow assessment, Sci. Total Environ. 774 (2021), 145005.

[22] D. Andriani, A. Wresta, T.D. Atmaja, A. Saepudin, A Review on optimization production and upgrading biogas through CO2 removal using various techniques, Appl. Biochem. Biotechnol. 172 (2014) 1909–1928.

[23] S.A. Orszag, V. Yakhot, W.S. Flannery, F. Boysan, D. Choudhury, J. Maruzewski, B. Patel, Renormalization Group Modeling and turbulence simulations. International Conference on Near-Wall Turbulent FlowsTempe, Arizona, 1993.

[24] R. Clift, J.R. Grace, M.E. Weber, Bubbles, Drops, and Particles, Academic Press, New York, 1978.

[25] A.W. Etchells, C.F. Meyer, Mixing in pipelines, in: Handbook of Industrial Mixing, 2003, pp. 391–477.

[26] A. Kukuková, B. Noël, S.M. Kresta, J. Aubin, Impact of sampling method and scale on the measurement of mixing and the coefficient of variance, AIChE J 54 (2008) 3068–3083.

[27] B.P. Leonard, S. Mokhtari, ULTRA-SHARP nonoscillatory convection schemes for high-speed steady multidimensional flow, NASA Lewis Research Center, United States, 1990.

[28] A. Fluent, ANSYS Fluent Theory Guide, Release 18.0. Ansys, Inc, 2017.

[29] K. Karim, R. Varma, M. Vesvikar, M.H. Al-Dahhan, Flow pattern visualization of a simulated digester, Water Res. 38 (2004) 3659–3670.

[30] A.M. Mendoza, T.M. Martínez, V. Fajardo, Modeling flow inside an anaerobic digester by CFD techniques, Internat. J. Energy Environ. 2 (2011) 963–974.

[31] M.S. Vesvikar, R. Varma, K. Karim, M. Al-Dahhan, Flow pattern visualization in a mimic anaerobic digester: experimental and computational studies, Water Sci. Technol. 52 (2005) 537–543.

[32] H. Lamb, Hydrodynamics, 6th Edition, 6th Edition ed., Cambridge university press1994.

[33] J. Kim, C. Park, T.-H. Kim, M. Lee, S. Kim, S.-W. Kim, J. Lee, Effects of various pretreatments for enhanced anaerobic digestion with waste activated sludge, J. Biosci. Bioeng. 95 (2003) 271–275.

[34] J. Zhang, N. Li, X. Dai, W. Tao, I.R. Jenkinson, Z. Li, Enhanced dewaterability of sludge during anaerobic digestion with thermal hydrolysis pretreatment: New insights through structure evolution, Water Res. 131 (2018) 177–185.

[35] J.L. Lumley, Turbulence in Non-Newtonian Fluids, Phys. Fluids 7 (1964) 335–337.

[36] A. Esmael, C. Nouar, A. Lefèvre, N. Kabouya, Transitional flow of a non-Newtonian fluid in a pipe: Experimental evidence of weak turbulence induced by shear-thinning behavior, Phys. Fluids 22 (2010), 101701.

[37] S. Rahgozar, D.E. Rival, On turbulence decay of a shear-thinning fluid, Phys. Fluids 29 (2017), 123101.

[38] H.O. Buhr, J.F. Andrews, The thermophilic anaerobic digestion process, Water Res. 11 (1977) 129–143.

[39] G.D. Gebreeyessus, P. Jenicek, Thermophilic versus mesophilic anaerobic digestion of sewage sludge: A comparative review, Bioengineering 3 (2016) 15.

[40] M.J. McFarland, Biosolids Engineering, McGraw-Hill Education, 2001.

[41] J.R. Stukenberg, J.H. Clark, J. Sandino, W.R. Naydo, Egg-shaped digesters: from Germany to the U.S, Water Environ. Technol. 4 (1992) 42–51.

[42] U. EPA, Process design manual for sludge treatment and disposal, Center for environmental research in formation technology transfer, (1979), pp.